Laser Ablation Mass Spectrometer (LAMS) as a Standoff Analyzer in Space Missions for Airless Bodies

X. Li [a,*], W. B. Brinckerhoff [b], G. G. Managadze[c], D. E. Pugel[b], C. M. Corrigan[d], J. H. Doty[e]

[a] *Center for Research and Exploration in Space Science & Technology, University of Maryland Baltimore County, 1000 Hilltop Circle, Baltimore, MD 21250, USA*

[b] *NASA Goddard Space Flight Center, 8800 Greenbelt Road, Greenbelt, MD 20771, USA*

[c] *Space Research Institute (IKI), Moscow, Russia*

[d] *National Museum of Natural History, Washington, DC, USA*

[e] *Rice University, Houston, TX, USA*

Abstract

A laser ablation mass spectrometer (LAMS) based on a time-of-flight (TOF) analyzer with adjustable drift length is proposed as a standoff elemental composition sensor for space missions to airless bodies. It is found that the use of a retarding potential analyzer in combination with a two-stage reflectron enables LAMS to be operated at variable drift length. For field-free drift lengths between 33 cm to 100 cm, at least unit mass resolution can be maintained solely by adjustment of internal voltages, and without resorting to drastic reductions in sensitivity. Therefore, LAMS should be able to be mounted on a robotic arm and analyze samples at standoff distances of up to several tens of cm, permitting high operational flexibility and wide area coverage of heterogeneous regolith on airless bodies.

Miniature mass spectrometers have been designed for use on space missions for decades [1-5]. Time-of-flight mass spectrometry (TOF-MS) has attracted increasing attention [6-10] due to its relative simplicity, wide mass range, high resolution, and compatibility with a variety of sampling and ionization methods. These advantages are especially beneficial on landed missions to airless bodies such as asteroids, comets, and most planetary satellites including the Moon. On such missions, a fixed lander or a rover may be deployed to explore a local region of the surface, where chemical analysis of a variety of regolith materials is expected to be a top priority. A laser ablation TOF-MS can be used for this analysis, without requiring collection and manipulation of samples [8, 9, 11]. In the laser ablation mass spectrometer (LAMS) instrument described previously [8, 9], a high-intensity pulsed laser is directed onto a sample of interest, forming ions that travel across the vacuum gap between the instrument and the analyzer inlet, and are subsequently focused in a reflectron. Normally, the gap distance L_{ext} (several cm in LAMS) has been treated as fixed, which would require precise instrument positioning such as with a robotic arm. However, it has been long known that the technique is compatible with variable L_{ext}. The Phobos probe carried the LIMA-D experiment [12], which was designed to operate from a hovering spacecraft, with $L_{ext} > 30$ m. Other types of mass analyzers, such as a hybrid ion trap TOF-MS [13] and a linear electric field (LEF) TOF-MS [14, 15] have been adapted for surface operations and tested in standoff mode, with L_{ext} of several meters. Here we describe an application of a simple LAMS for fine-scale *in situ* analysis of samples at variable L_{ext} up to at least several tens of cm, compatible with a robotic arm deployment (Figure 1) for access to many m^2 around a lander or rover. As shown in Figure 1, the field-free drift length L is the sum of ion path lengths outside (L_{ext}) and inside (L_{int}) the spectrometer. We show via theoretical simulation that high mass resolution ($R > 250$, sufficient to resolve unit mass isotopes) elemental analysis can be achieved for L ranging from 33 cm to at least 100 cm.

In the LAMS design as described previously [8], the laser ablated ions travel from the sample surface into the mass analyzer and are redirected in a two-stage reflectron onto a dual microchannel plate (MCP) detector, arriving at a sequence of times proportional to the square root of their mass-to-charge ratios, i.e., $(m/z)^{1/2}$. Neglecting the initial temporal and spatial spreads, the TOF of a particle with mass m and initial kinetic energy zV is given by the following equation (1):

$$2 \quad 12 = 12+4\ 1\ 1\ 12- - 112+4\ 2\ 2- 1(-1)1/2+2(1+ 2) \quad [1/2 - (-)1/2]+ 2\ 3| \ | \ [(-)1/2- 1/2] \quad (1)$$

The voltages V_1 and V_2 are applied to grids defining reflectron stages of lengths d_1 and d_2, respectively. A retarding potential analyzer (RPA) in front of the detector, with analyzer voltage V_A applied between grids separated by distances a_1 and a_2 defines a minimum kinetic energy that ions must exceed to reach the microchannel plate (MCP) detector, which is separated from the RPA by gap a_3 and held at negative voltage V_D for positive ions. Neglecting the last very small term, equation (1) is reduced to

$$21/2 \ / \approx 1\ 1/2+4\ 1\ [1/2-(-)1/2]+4\ 21-(-)1/2+2(1+ 2) \quad [1/2 - (-)1/2] \quad (2)$$

where $\tau = (2z/m)^{1/2}t$, $p = V/V_2$, $c = V_1/V_2$, $q = V_A/V_2$, $\delta_1 = d_1/L$, $\delta_2 = d_2/L$, $\alpha_1 = a_1/L$ and $\alpha_2 = a_2/L$. By additionally neglecting the last term of (2), representing the relatively short time ions spend in the RPA, a second-order reflectron focus at $c \approx 0.6$ was identified and verified experimentally to provide acceptable resolution at the fixed $L = 33$ cm [8] for a wide range of $V_A > V_1$. The detected initial kinetic energy (IKE) band, determined by $V_2 - V_A$, was typically set as large as possible to maximize sensitivity, however, a resolution dependence on V_A was noted resulting in frequent empirical adjustment. Aside from the increase in resolution obtained, in principle, as V_A approaches V_2, there is in fact a single local maximum in the resolution for relatively large energy window, when the last term of (2) is taken into account. Moreover, when considering variable L, identifying the specific values of c and q as a function of L allows acceptable resolution and sensitivity to be recovered at arbitrary L_{ext}, as described in the calculations below.

The LAMS mass resolution was determined and optimized as a function of L, c, and q using a one-dimensional model based on the scaled TOF given by (2). IKEs (p) were scanned over the selected range of $1 > p > q > c > 0.5$, corresponding to ions turning around in the second

stage of the reflectron and traversing the RPA. The resolution given by $R = m/\Delta m = t/2\Delta t = \tau/2\Delta\tau$, where τ is taken as the midpoint, and $\Delta\tau$ is taken as the width, of the scaled TOF range given by (2) over all values of p. The full width at half maximum (FWHM) of the TOF peak is typically taken as Δt, whereas here, the calculated R corresponds most closely to the base peak resolution, giving a conservative lower bound for the actual instrument.

Using L = 33 cm as an example, Figure 2(a) shows the plot of the calculated results when $V_A = V_1$ ($q = c$). The p value ranges linearly from 0.502 to 0.992, in 0.01 steps. The red dotted line marks the focus point where c = 0.594 and the mass resolution is found to be 39.76. By increasing q, the energy window becomes narrower and narrower, that is, fewer ions reach the detector. The mass resolution increases with q until it reaches a local maximum, and then decreases again. Figure 2(b) shows the plot where the maximum resolution is achieved with optimal V_A, and a clear resultant shift of c is observed as shown in Figure 2(c). In that condition, the calculation suggests a maximum resolution of R = 286.43 can be achieved when q = 0.651 and c = 0.610, around 7 times the resolution of the $V_A = V_1$ case. The calculated results have been plotted in Figure 3(a) as a contour plot of resolution, q and c, where two maximum areas are observed. In addition, at the total length of 33 cm, the best resolution is found within a very narrow Δq range, such that in practice coarse tuning of V_A could easily miss the optimized condition. However, the calculated Δq for mass resolution R = 250 is around 0.02. It means for example, at the condition of V_2 = 100 V, a still good resolution-if not the maximum-can be achieved by tuning V_A within a voltage range of 100 x 0.02= 2 V, which is experimentally reasonable.

Using the same method, we have extended our simulations to varied lengths, i.e., L = 34 cm, 36 cm, 38 cm, 40 cm, 60 cm, 80 cm, and 100 cm. The results for varied length of the optimized (optimal V_A) focus of c and resolution are listed in Table 1, and a contour plot of resolution, q and c for L = 100 cm is shown in Figure 3(b). Representative plots, the resolution, and $V_2^{1/2}\tau$ / L values plotted as a function of L are shown in Figure 4. It can be seen that with the length increasing, the optimized (best focus) c value increases, with the resolution increasing substantially. For example, when L = 60 cm, the optimized resolution increases to $R \approx 483$, and when L = 100 cm, the optimized resolution becomes $R \approx 912$ (in practice, R may not exceed ~600 due to space charge in the ion plume). Note from the case of L = 100 cm, q reaches ~ 0.9 at

the optimal c value as shown in Table 1, which indicates the sensitivity would be reduced at relatively large L. However, the practical resolution requirement of $R > 250$ can be achieved at a wider energy window with higher sensitivity ($q \sim 0.85$ in the case of $L = 100$ cm). Furthermore, at larger L the resolution is less sensitive to uncertainties in c and q; conversely at fixed c and q the resolution is less sensitive to uncertainty in L which is beneficial at large L.

Above all, LAMS should be able to maintain $R > 250$ over a range of L up to at least 1 m. It is worth making note of how the accommodation of this range could be implemented on a realistic lander or rover mission to an airless body. The primary challenge to overcome, assuming adequate resolution, is the loss of ion density with increasing L_{ext}. The density can conservatively be assumed to fall off as L_{ext}^{-2}, although the "beaming" behavior of high-intensity laser ionization would likely soften this somewhat. As an example, for an instrument configured with $L_{ext} = L - 25$ cm, the ion density at $L = 100$ cm would be ~1% of that at $L = 33$ cm. This factor is not unmanageable within the resources available to a landed mission, given the ability of LAMS to generate very high ion densities. In normal operation, the laser energy and spot size are deliberately limited so as not to produce signals that can saturate the microchannel plate detector on major elements in as little as one laser pulse. Operating without such limitations and integrating over a larger number of pulses are expected to compensate for the loss of ion density at longer stand-off distances. A second challenge would be accommodating the variable range to target, which requires maintaining a small laser spot at different distances, and knowledge of L_{ext} for instrument calibration. This is best handled through a combined focusing protocol, where the approximate distance, determined through imaging autofocus, is used to position the laser objective lens. Then final determination of L_{ext} is achieved by varying laser energy and optimizing LAMS spectra over a small range of c and q. A third challenge is the uncertainty in the surface morphology of the target sample, which is the case for all distances but may be greater at larger L_{ext}. Fortunately, the LAMS technique is sufficiently "destructive" on the local scale to create a small ablation pit that tends to orient toward the incoming laser beam within a few (5-20) initial high-energy pulses. After this "pre-ablation" step, irregularities in the sample surface may be removed with ions then emitted generally toward the LAMS inlet.

The results of the calculations given here are sufficiently encouraging that we are in the process of developing an appropriate laboratory demonstration of LAMS over the distances

modeled, using a set of realistic target samples. The use of a variable-standoff LAMS may thus be a potentially powerful and flexible tools for *in situ* measurements of the heterogeneous surface compositions of airless bodies.

Acknowledgement

This work was supported by the NASA Planetary Instrument Definition and Development (PIDDP) program and by the Goddard Internal Research and Development program.

Tables

Table 1: As a function of detection lengths, the calculated c, resolution and $V_2^{1/2}\tau/L$ values with $V_A = V_1$, and calculated q, c, resolution and $V_2^{1/2}\tau/L$ values with optimal $V_A > V_1$.

	$V_A = V_1$			*Optimal* $V_A > V_1$			
L(cm)	**$c=V_1/V_2$**	**Resolution**	**$V_2^{1/2}$ t/L**	**$q=V_A/V_2$**	**$c=V_1/V_2$**	**Resolution**	**$V_2^{1/2}$ t/L**
33	0.594	39.76	1.626	0.651	0.610	286.43	1.633
34	0.594	39.68	1.614	0.660	0.616	287.94	1.618
36	0.604	39.55	1.587	0.673	0.626	304.87	1.591
38	0.614	39.70	1.558	0.693	0.638	302.60	1.569
40	0.624	36.96	1.538	0.702	0.646	323.32	1.545
60	0.684	33.55	1.392	0.802	0.718	483.44	1.402
80	0.726	33.01	1.314	0.864	0.764	676.48	1.326
100	0.756	34.87	1.265	0.903	0.796	912.71	1.278

Figure Captions

Figure 1. A Laser Ablation Mass Spectrometer (LAMS) with variable standoff capability may be implemented on an airless body surface mission to analyze the elemental composition of samples around the lander. $L = L_{int} + L_{ext}$ is the total field free drift distance of the laser ablated ions.

Figure 2. At L = 33 cm, adjusting the analyzer voltage V_A from (a) the "wide window" case $V_A = V_1$ to (b) an optimal $V_A > V_1$ results in an effectively higher order focus (higher resolution) without having to significantly reduce the ions (represented by the number of trajectory curves) that reach the detector. Optimizing V_A shifts the reflectron focus c slightly as shown in (c).

Figure 3. Contour plots of the resolution as a function of c and q show the distinct local maximum at L = 33 cm (a) with a relatively wide window (V_2-V_A) whereas at L = 100 cm (b) high resolution (R > 250) is achieved over a wider range of c and q, but with a smaller window.

Figure 4. (a) Scaled time of flight plots show the position of the focus $c = V_1/V_2$ and the set of ion kinetic energies at the maximum mass resolution (optimal V_A), for different values of L. (b) Plot shows the focus $c = V_1/V_2$ in inverse proportion vs. scaled TOF points at maximum resolution, and the fitting line indicates a linear relationship between them.

References

1. Rushneck, D.R., A.V. Diaz, D.W. Howarth, J. Rampacek, K.W. Olson, W.D. Dencker, P. Smith, L. McDavid, A. Tomassian, M. Harris, K. Bulota, K. Biemann, A.L. LaFleur, J.E. Biller, and T. Owen, Viking gas chromatograph--mass spectrometer. Review of Scientific Instruments. 49 1978, 817-834.
2. Niemann, H.B., D.N. Harpold, S.K. Atreya, G.R. Carignan, D.M. Hunten, and T.C. Owen, Galileo Probe Mass Spectrometer experiment. Space Science Reviews. 60 1992, 111-142.
3. Niemann, H.B., J.R. Booth, J.E. Cooley, R.E. Hartle, W.T. Kasprzak, N.W. Spencer, S.H. Way, D.M. Hunten, and G.R. Carignan, Pioneer Venus Orbiter Neutral Gas Mass Spectrometer Experiment. Geoscience and Remote Sensing, IEEE Transactions on. GE-18 1980, 60-65.
4. Balsiger, H., K. Altwegg, P. Bochsler, P. Eberhardt, J. Fischer, S. Graf, A. Jäckel, E. Kopp, U. Langer, M. Mildner, J. Müller, T. Riesen, M. Rubin, S. Scherer, P. Wurz, S. Wüthrich, E. Arijs, S. Delanoye, J. Keyser, E. Neefs, D. Nevejans, H. Rème, C. Aoustin, C. Mazelle, J.L. Médale, J. Sauvaud, J.J. Berthelier, J.L. Bertaux, L. Duvet, J.M. Illiano, S. Fuselier, A. Ghielmetti, T. Magoncelli, E. Shelley, A. Korth, K. Heerlein, H. Lauche, S. Livi, A. Loose, U. Mall, B. Wilken, F. Gliem, B. Fiethe, T. Gombosi, B. Block, G. Carignan, L. Fisk, J. Waite, D. Young, and H. Wollnik, Rosina – Rosetta Orbiter Spectrometer for Ion and Neutral Analysis. Space Science Reviews. 128 2007, 745-801.
5. Mahaffy, P., Exploration of the Habitability of Mars: Development of Analytical Protocols for Measurement of Organic Carbon on the 2009 Mars Science Laboratory Strategies of Life Detection, O. Botta, J.L. Bada, J. Gomez-Elvira, E. Javaux, F. Selsis, and R. Summons, Editors. 2008, Springer US. p. 255-268.
6. Scherer, S., K. Altwegg, H. Balsiger, J. Fischer, A. Jäckel, A. Korth, M. Mildner, D. Piazza, H. Reme, and P. Wurz, A novel principle for an ion mirror design in time-of-flight mass spectrometry. International Journal of Mass Spectrometry. 251 2006, 73-81.
7. Getty, S.A., I.L. ten Kate, S.H. Feng, W.B. Brinckerhoff, E.H. Cardiff, V.E. Holmes, T.T. King, M.J. Li, E. Mumm, P.R. Mahaffy, and D.P. Glavin, Development of an evolved gas-time-of-flight mass spectrometer for the Volatile Analysis by Pyrolysis of Regolith (VAPoR) instrument. International Journal of Mass Spectrometry. 295 2010, 124-132.
8. Brinckerhoff, W.B., G.G. Managadze, R.W. McEntire, A.F. Cheng, and W.J. Green, Laser time-of-flight mass spectrometry for space. Review of Scientific Instruments. 71 2000, 536-545.
9. Brinckerhoff, W.B., On the possible in situ elemental analysis of small bodies with laser ablation TOF-MS. Planetary and Space Science. 53 2005, 817-838.
10. Hohl, M., P. Wurz, S. Scherer, K. Altwegg, and H. Balsiger, Mass selective blanking in a compact multiple reflection time-of-flight mass spectrometer. International Journal of Mass Spectrometry. 188 1999, 189-197.
11. Urs, R., A.W. James, and W. Peter, A miniature laser ablation time-of-flight mass spectrometer for in situ planetary exploration. Measurement Science and Technology. 14 2003, 2159.
12. Managadze, G.G. and I.Y. Shutyaev, *Chapter 5 in Laser Ionization Mass Analysis*, 1993, Wiley: New York.
13. De Young, R.J. and W. Situ, Elemental Mass Spectroscopy of Remote Surfaces from Laser-Induced Plasmas. Applied Spectroscopy. 48 1994, 1297-1306.
14. Wiens, R.C., D.A. Cremers, J.D. Blacic, H.O. Funsten, and J.E. Nordholt, *Stand-off planetary surface analysis using laser-induced breakdown spectroscopy and laser-induced plasma ion mass spectrometry*, in *In Situ Resource Utilization (ISRU II) Technical Interchange Meeting*1997. p. 37-39.

15. Wiens, R.C., D.A. Cremers, J.D. Blacic, S.M. Ritzau, H.O. Funsten, and J.E. Nordholt, *Elemental ans isotopic planetary surface analysis at stand-off distances using laser-induced breakdown spectroscopy and laser-induced plasma ion mass spectrometry.*, in *Lunar and Planetary Science XXIX*1998. p. 1633.

Figures

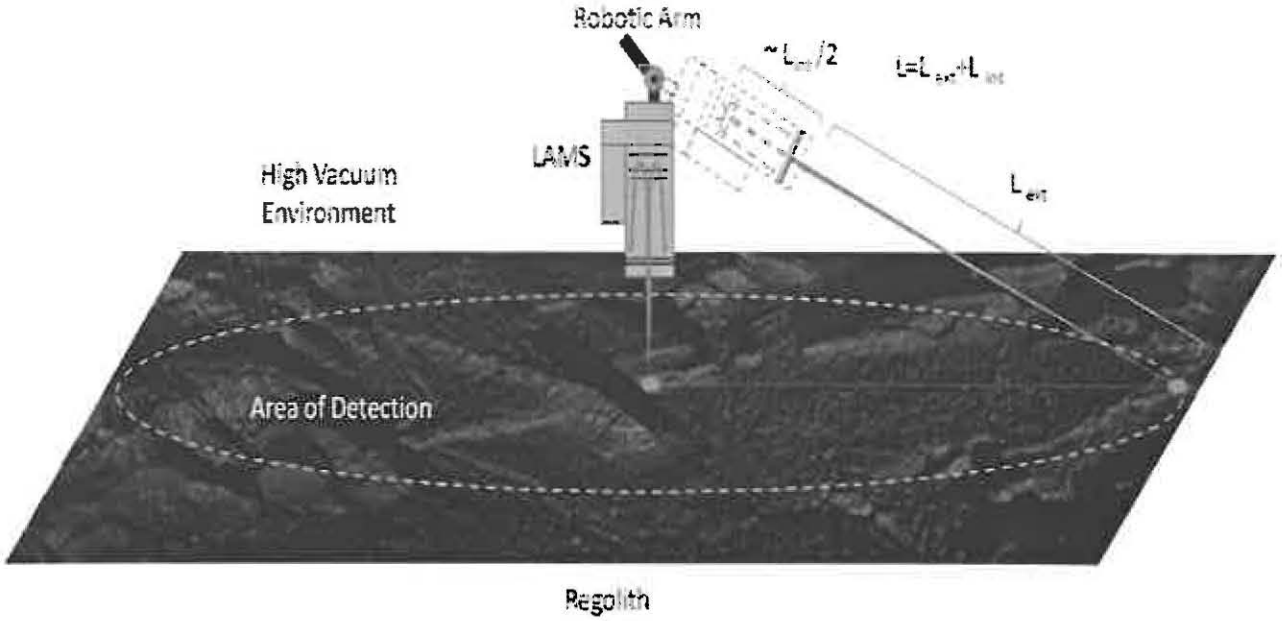

Figure 1

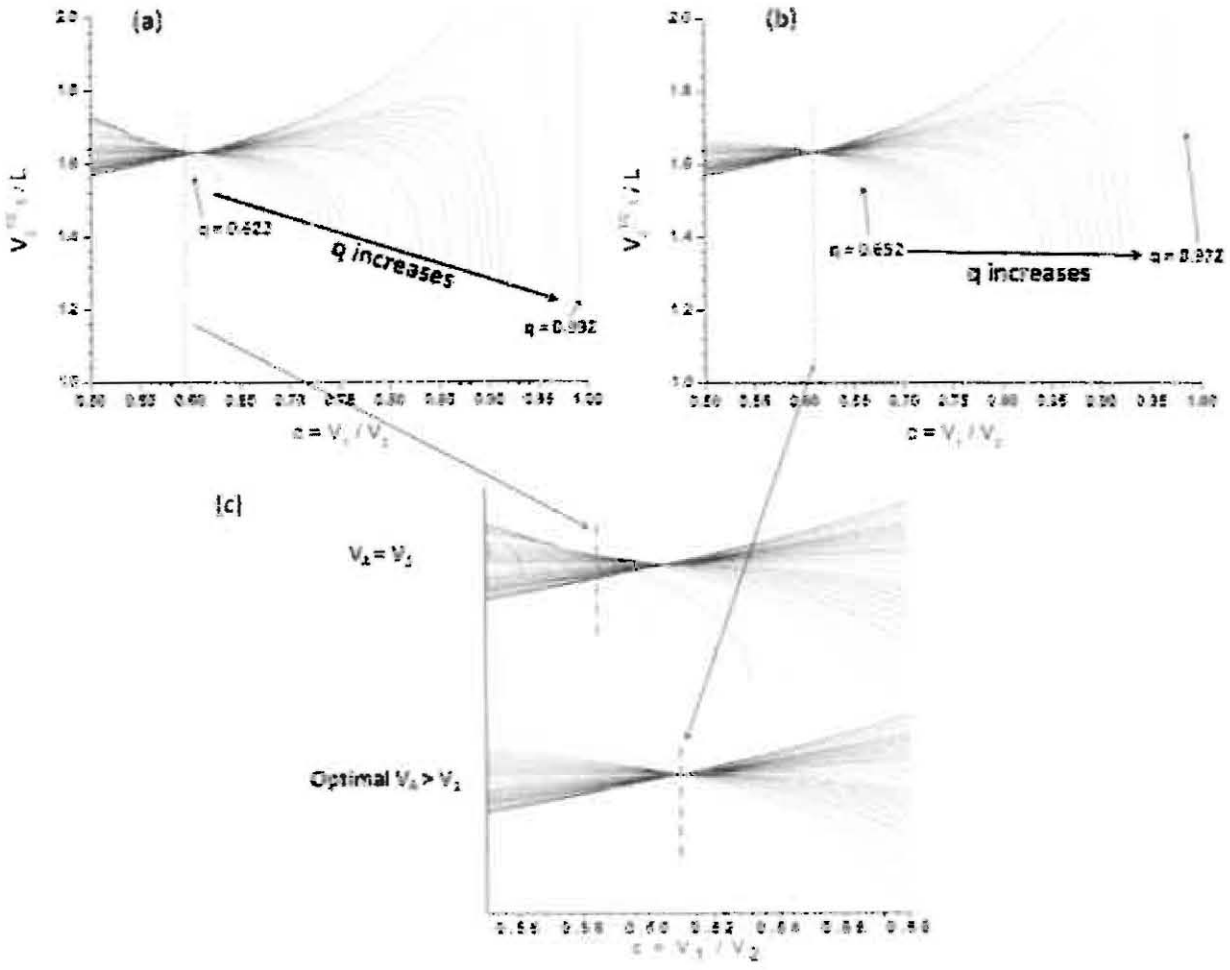

Figure 2

(a) L=33cm

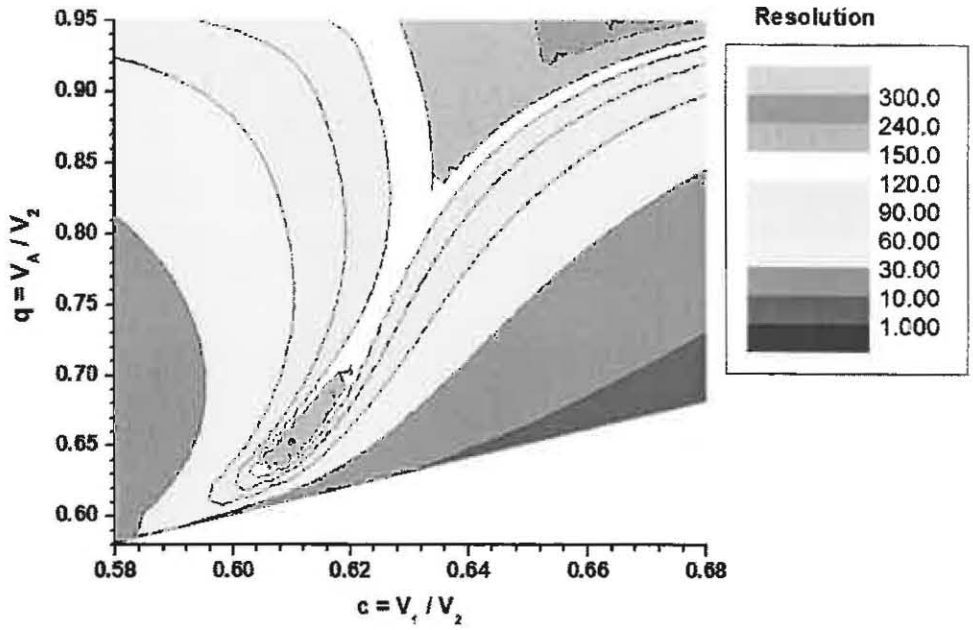

(b) L=100cm

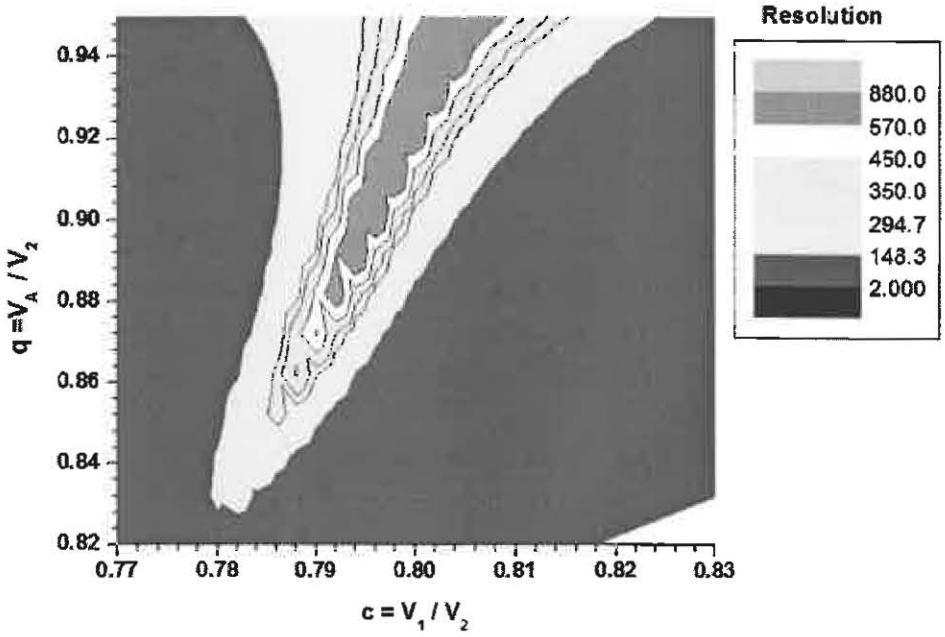

Figure 3

(a)

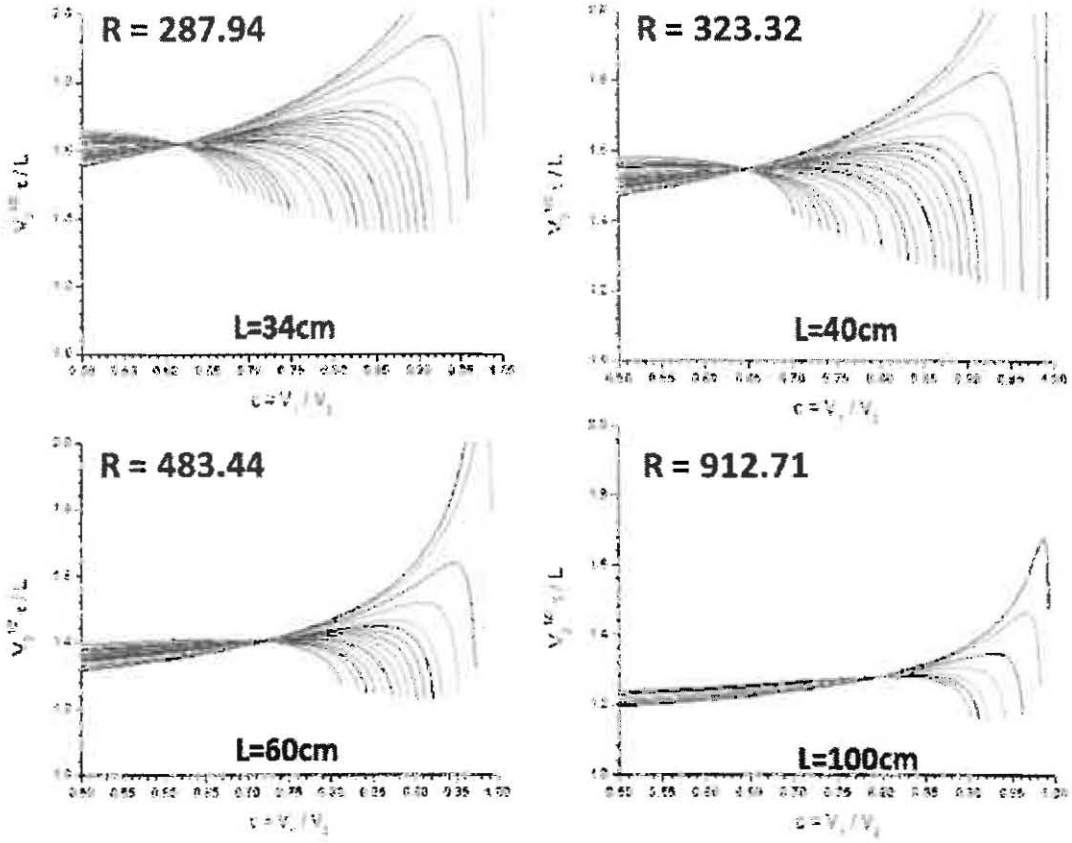
R = 287.94
L=34cm
R = 323.32
L=40cm
R = 483.44
L=60cm
R = 912.71
L=100cm

(b)

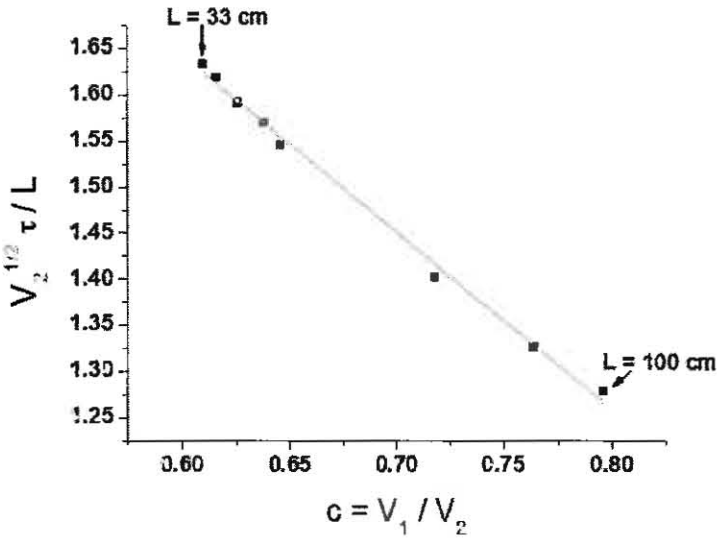
L = 33 cm
L = 100 cm
1.65
1.60
1.55
1.50
1.45
1.40
1.35
1.30
1.25
0.60
0.65
0.70
0.75
0.80
c = V1 / V2

Figure 4